Chapter 3 - Dendritic remodeling but not sub-dendritic GABAergic synapse targeting is affected by blocking chloride channels during postembryonic motoneuron development

3.1 Abstract

Assembling neurons appropriately into neuronal circuits requires specific changes in neuronal geometry, membrane properties and synaptic connectivity. In holometabolous insects the postembryonic acquisition of novel behavioral functions is accompanied by well described changes in dendritic architecture and physiological properties of identified motoneurons. We have recently demonstrated that postembryonic remodeling of dendritic shape is accompanied by stereotyped rules for sub-dendritic distribution of GABAergic synapses. Here we ask whether $GABA_A$ like receptor mediated chloride influx affects dendritic architecture and sub-dendritic synapse targeting. PTX induced blockade of chloride ion influx causes dendritic overgrowth, affects the amount of GABAergic terminals impinging on the dendritic tree, whereas the distribution pattern of these terminals remains unaltered. Behavioral testing reveals that these neuronal changes modify the animal's ability to fly.

3.2 Introduction

Dendritic architecture of central neurons is crucial to ensure connections with the correct synaptic partners, and it affects synaptic input integration of individual neurons (Connors and Regehr, 1996; Häusser et al., 2000; Vetter et. al, 2001). Therefore, dendritic shape is important for adequate neural network function. During development, dendritic shape is regulated by innate genetic factors (Montague and Friedlander, 1989; 1991; Spatkowski and Schilling, 2003; Gao and Bogert, 2003; Mizrahi et al., 2000; Scott et al., 2002; Scott et al., 2003), external molecular cues (Kim and Chiba, 2004; Landgraf and Thor, 2006) humoral cues such as growth factors and hormones (Torran-Allerand et al., 1999; Weeks and Levine, 1995; Cooke and Wooley, 2005) and by neuronal activity (Hofer et al., 2006; Duch and Mentel, 2004; Libersat and Duch, 2004; Wong and Gosh, 2002). This study addresses the role of GABA mediated inhibition, causing chloride influx, for the development of dendritic architecture of an identified motoneuron during the metamorphosis of the moth, *Manduca sexta*.

Insect metamorphosis offers a useful model to study mechanisms underlying behaviorally relevant modifications of dendritic architecture during postembryonic development, because individually identified neurons acquire their behavioral function, their geometry and their physiology during the transformation from the larval into the adult stage (Consoulas et al., 2000). Dendritic and functional remodeling has been described in particular detail for the motoneuron 5, MN5, in *Manduca sexta*. During metamorphosis MN5 develops from a slow larval crawling motoneuron into a fast adult flight motoneuron. To accommodate this functional change, MN5 is remodeled with respect to its physiological properties, its synaptic partners and its dendritic architecture. Dendritic architecture changes, synapse disassembly and re-assembly, synaptogenesis on dendritic filopodia and postembryonic ionic current modifications have been analyzed quantitatively by means of 3-D reconstructions, novel co-localization analysis tools, *in situ* voltage clamp and imaging experiments (Duch and Levine, 2000; 2002; Libersat and Duch, 2002; Mentel and Duch, 2004; Evers et al., 2005; 2006). Multi-compartment modeling analysis suggests that dendritic architecture remodeling causes dendritic shape changes that underlie behaviorally relevant computational properties of the dendritic tree (Meseke et al., unpublished). Moreover, a recent study demonstrates that postembryonic dendritic remodeling of MN5 is accompanied distinct changes in sub-dendritic targeting of putative GABAergic inputs throughout the dendritic tree (Meseke et al., unpublished). While MN5 is transformed into a fast flight motoneuron, the distal dendrites receive a higher density of putative GABAergic inputs, and the roots of dendritic sub-trees are contacted by GABAergic terminals with a significantly higher likelihood than all other dendritic branches, whereas the larval crawling MN5 does not exhibit these sub-dendritic input synapse distribution characteristics.

Steroid hormones play a major role in postembryonic dendritic property regulation (Weeks and Levine, 1990; Levine and Weeks, 1996; Consoulas et al., 2000; Weeks, 2003), but activity has also been demonstrated to affect dendritic architecture and steroid induced synapse disassembly (Duch and Mentel, 2004; Burkert and Duch, 2006). Therefore, this study tested by systemic injections of the chloride channel blocker picrotoxin (PTX) whether $GABA_A$ receptor mediated inhibition affects the maturation of adult dendritic shape and sub-dendritic GABAergic synapse targeting. Site-specific targeting of synapses within dendritic trees is likely an intermediate step between genetically encoded axon guidance and experience dependent circuit refinement, and it is not clear whether GABAergic transmission is needed as an

instructive mechanism. Experience guided sub-cellular synapse elimination has been reported to confine inhibitory glycinergic inputs to the somata of auditory interneurons in rodents (Kapfer et al. 2002). By contrast, specific sub-cellular targeting of two different types of major GABAergic synapses along the perisomatic and the dendritic domains of pyramidal neurons in visual cortex (Freund and Buzsáki, 1996) does not rely on experience dependent thalamic input (Di Cristo et al., 2004). Here we demonstrate that PTX induced blockade of chloride influx affects distinct features of dendritic geometry, causes dendritic overgrowth, but does not affect the sub-dendritic targeting, but the amount of GABAergic terminals impinging on the dendritic tree of MN5. These neuronal alterations impair the animal's ability to fly only mildly.

3.3 Methods

3.3.1 Animals

Manduca sexta were obtained from our laboratory culture. Animals were reared on artificial diet (Bell and Joachim, 1976) under a long-day photoperiod regime (18/6 h light/dark cycle) at ~26°C. Both chronological and morphological criteria were used for staging of animals (Bell and Joachim, 1976; Reinecke et al., 1980; Tolbert et al., 1983). Dissection and intracellular recording were performed as described in Duch and Levine (2000).

3.3.2 Injections of pharmacological reagents

Overall neuronal excitability was altered during postembryonic development by systemic injections of either the sodium channel blocker tetrodotoxin (TTX, Sigma) or the chloride channel blocker picrotoxin (PTX, Sigma) at pupal stage P2. Both reagents were injected with a Hamilton syringe through the wing anlagen which can clearly be visualized on the outside pupal cuticle. Injection concentrations were 10^{-2} or 10^{-3} M in saline, and injection volumes were adjusted by total body weight to reach a final concentration of 10^{-5} M with respect to animal weight. This resulted in injection volumes of approximately 20 µl. To test for unspecific effects of the injection procedure, two types of control experiments were conducted. First, animals were not injected at all, and developmental time as well as reflex responsiveness was compared to injected animals. Second, animals were injected with the same volumes of saline and dendritic structure as well as synapse distributions were compared to PTX injected

animals. Following the injection at stage P2, no further injection injections were conducted. To avoid bleeding the wound was covered with bee wax and animals developed and molted to an adult moth.

To induce prolonged flight in behavioral experiments the octopamine agonist chlordimeform (CDM, Sigma) was injected into the abdomen of adult moths at concentration of 10^{-4} M and a volume of 20 µl. CDM is known to induce flight motor pattern and it has also been assigned to increase the responsiveness to sensory stimulation (Kinnamon et al., 1984). This pharmacological manipulation was used to induce maximum flight motor output in animals of various different experimental groups.

3.3.3 Behavioral testing

To monitor the effectiveness of neurotoxin injection experiments to induce changes in neuronal excitability, all animals included in this study were tested for the well described pupal gin-trap reflex. The gin-trap reflex is a strong abdominal deflection in response to mechanical stimulation of the gin-trap region located between adjacent abdominal segments (Lemon and Levine, 1997a; 1997b; Bate, 1973). PTX, TTX and control animals were tested daily for the presence or absence of the gin-trap reflex. The number of abdominal movements that was induced by a single mechanical stimulation was counted and averaged over 5 five stimuli per animal per day.

To test whether injections of PTX at pupal stage P2 had any effect on adult flight performance, the following flight parameters were measured in behavioral tests: (i) the percentage of animals which showed flight behavior, the total flight duration and wing beat frequency. All animals subjected to flight behavioral experiments were one day old. They were immobilized by chilling on ice for 20 minutes. Scales were shaved off their ventral thorax and the shaved part of the cuticle was carefully cleaned with 50 % ethanol to create a clean surface that allowed gluing animals to a wooden stick with UHU (Two component gluten, UHU GmbH; Bühl, Germany). Animals were allowed to recover from cold anesthesia for 45 minutes at 22°C and afterwards softly stimulated to induce a warm up phase – the time the moths only shake their wings inappropriately to fly but to warm up their muscles for flight. Then, animals were fixed in a flight-like position in a stand with their wings free to move. Flight was induced by applying a wind stimulus with a cold hair dryer fixed to a stand at distance of 40 cm (Phillips professional 1600 cool). Wind stimulation was switched-off as soon as the moth started

flying. Brief wind stimuli were re-applied as soon as an animal stopped flying. The experiment was terminated as soon as three consecutive wind stimuli did not induce any flight motor behavior. Flight was filmed with a digital high speed camera (1000 pictures per second; Motion Scope; Redlake Imaging; Morgan Hill, CA) placed in front of the animal in approximately 30-40 cm distance. This allowed a detailed analysis of the flight behaviour by determining the wing beat frequency as well as the flight duration. Flying moths were filmed for 3 seconds each after the first, the 15th and the 30th. Data files were stored on a personal computer for analysis. All behavioral experiments were conducted as blind tests, i.e. the experimenter was unaware of the treatment group of the animals.

3.3.4 Intracellular labelling and immuncytochemistry

Intracellular staining of MN5 and subsequent sample preparation was achieved as described in Duch and Levine (2000) and Evers et al. (2006). Briefly, for intracellular labeling of MN5 a thin walled glass microelectrode (25-35 MΩ tip resistance) was filled with a mixture of 7 % Neurobiotin (Linaris GmbH, Wertheim-Bettingen, Germany) and Rhodamin-Dextran (Invitrogen, Carlsbad, CA, USA) in 2 M potassium acetate. An air bubble was left between the dye filled tip and the shaft filled with 2 M potassium acetate to avoid dye dilution. Following intracellular penetration of MN5 (identified by antidromic spike initiation via extracellular nerve 1 stimulation) the dyes were injected ionophoretically by a constant depolarizing current of 3 nA for 45 to 60 minutes. Then the electrode was removed, the ganglia were fixed in 4% paraformaldehyde in phosphate-buffer solution (PBS, 0.1M) for 2 h at room temperature. Ganglia were washed in PBS (0.1M) six times for 15 minutes each. Then tissue was treated in a conventional microwave at 750 W for 5 times at 4° C to enhance antibody penetration and binding. This was followed by additional 2 washes in 0.1 M PBS for 15 minutes each and dehydration in an ethanol-series (50, 70, 90, and 2 times 100 %, 15 minutes each). Preparations were treated in a 1:1 mixture of pure ethanol and methyl salicylate for 5 minutes and cleared in methylsalicylate. This was followed by 5 minutes treatment in a 1:1 mixture of pure ethanol and methyl salicylate, rehydration in a descending ethanol series, 4 washes in PBS-triton x (0.5 % triton in 0.1 M PBS). Primary antibody incubation with anti-SynapsinI (SynOrf1, kindly provided by Prof. Buchner, University Würzburg; 1:100) and anti-GABA (Sigma-Aldrich Chemie GmbH, Schnelldorf, Germany; 1:400) were conducted for 36 hours in PBS-triton x (0.3 %). This was

followed by 6 washes in PBS (15 minutes each) and incubation with secondary antibodies. Neurobiotin was visualized with Cy2-streptavidin (Invitrogen, Karlsruhe, Germany; 1:750); GABAergic processes were visualized by incubation with Cy3-coupled mouse anti-Rabbit (Jackson Immunochemicals Inc., Suffolk, UK; 1:200), and synaptic terminals were visualized by incubation with Cy5-coupled rabbit anti-Mouse antibody (Jackson Immunochemicals Inc.; 1:200). This was followed by 6 washes in PBS (0.1 M), dehydration in an ethanol series (see above), 5 minutes treatment in a 1:1 mixture of pure ethanol and methyl salicylate and clearing and mounting in methyl salicylate.

3.3.5 Data acquisition

Images were acquired with a Leica TCS SP2 confocal laser scanning microscope (Bensheim, Germany) using a Leica HCX PL APO CS 40x oil immersion objective (numerical aperture 1.25). To prevent crosstalk between overlapping fluorescent emission wavelength sequential scanning mode was used. Cy2 and Cy5 were scanned simultaneously by using excitation wavelengths of 488 nm (argon laser) and 633 nm (helium neon laser). Cy2 emission was detected between 495 and 530 nm, and Cy5 emission was detected between 640 and 670 nm. No cross-talk between the channels was detected. Cy3 was excited with a green neon laser at 543 nm and detection wavelength was between 550 and 590 nm. Switching between Cy3 scanning and Cy2/Cy5 scanning was conducted after every frame.

By optimizing the sample preparation procedure as described previously (Evers et al., 2005), we can discriminate structures with a diameter of below the emitting wavelength, approaching the theoretical limit of half the emitting wavelength (300 nm), at least in *XY* (Evers et al., 2005; 2006). The smallest dendritic diameters we find in MN5 are above 400 nm diameter. Electron microscopy of Manduca thoracic motor neuropil at the developmental stages relevant for this study demonstrates that synapsin I immunolabeled synaptic terminals appear as distinct puncta of 300 to 3000 nm diameter (Hohensee et al., 2007). Therefore, precise 3-dimensional reconstructions of dendritic surface (see below) can be used to map the distribution of immunolabled synaptic terminals onto the dendrites of identified motoneurons.

3.3.6 Image analysis

Confocal image stacks were further processed with Amira-3.1.1 software (TGS). For 3-dimensional reconstruction of dendritic segments software plugins as published previously (Schmitt et al., 2004; Evers et al., 2005) were used. These deliver precise quantification of midline and diameter as well as a triangulated surface definition fully exploiting optical resolution. To address the distribution of putative input synapses into the dendritic tree of MN5, immunolabeled synaptic profiles were used. For quantification of the distribution of immunolabeled profiles along dendrites, the generated surface description was used to calculate the staining density within 300 nm from each surface element, a triangle. The position of the triangle was determined perpendicular to the midline of the corresponding reconstructed segment (for details see Evers et al., 2005). A recent electron microscopy study demonstrated that this procedure accounted for all synaptic terminals located in the thoracic motor neuropils of Manduca, but that it produced approximately 20 percent false positive synapses if only one immunolabel was used (Hohensee et al., 2007). In this study this procedure was done for two immunolabels, anti-synapsin-I and anti-GABA. The correlation of both was used to indicate sites of putative GABAergic input synapses. Snapshots of scenes rendered in Amira-3.1.1 are arranged into figures with Adobe Illustrator CS and Photoshop CS (Adobe Systems Incorporated).

3.3.7 Statistical analysis

For statistical analysis, morphological data sheets exported as CSV-tables generated in Amira 3.1.1 software (TGS) were imported into R (R Development Core Team, 2004), Microsoft Exel software and Statistica (StatSof, Hamburg, Germany). ANOVA with Duncan post hoc comparison are used to test for statistical differences between multiple groups, for example morphometric values as occurring in different Sholl spheres. Overall morphometric parameters were compared between manipulated and control adult motoneurons with Student's t-test.

Statistical analysis for flight time values and wing beat frequency was done with Kruskall-Wallis ANOVA and if significant differences between multiple groups were detected, Mann-Whitney U-Test's were performed to test two groups individually to each other. Box plots were chosen to display measurements with median and 25 to 75% quartile but no outliers with extreme values were shown.

3.4 Results

Time of pupal development is not altered by the injections procedure or by PTX action, because the developmental time course throughout pupal life is similar between non-injected, saline injected and PTX injected animals (Fig 1A). In addition injected animals showed a normal sequential appearance of external staging criteria throughout all stages of postembryonic development, and careful dissection of adults does not reveal any major differences with regard to major internal structure. All animals showed the full repertoire of motor behaviors. Therefore, injections do not have a major overall effect on development. Furthermore, reflex responsiveness to mechanical stimulation is not altered by the injection procedure because saline injected and non-injected animals show similar gin trap reflex responses throughout all stages of pupal development (Fig 1B). Injection of PTX at pupal stage P2 increased reflex responsiveness significantly (Fig 1B). Increased responsiveness upon systemic PTX injection is observed throughout all stages of pupal development (Fig 1B), clearly demonstrating that neuronal excitability is increased, and that this effect holds for up to three weeks of pupal

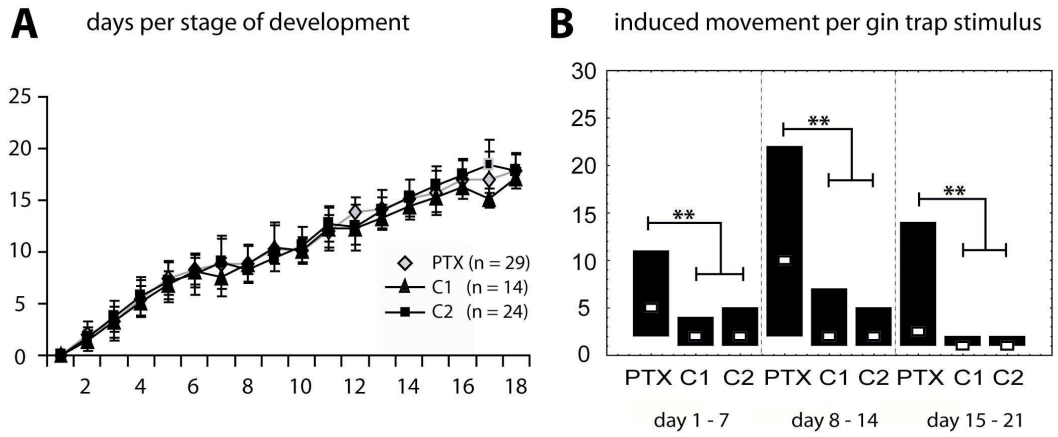

Figure 1. *Inluences of drug injection on developmental time during metamorphosis and neuronal excitability by stimulation of the gin trap reflex*
(A) shows the mean number of days needed for pupal development at a given stage for animals without injection (C1, black triangle), with injection of saline (C2, black squares) and PTX injected animals (PTX, grey square). Time of pupal development is not altered by any of these manipulations. (B) shows the responsiveness to mechanical stimulation of the gin trap region, a reflex. Postembryonic development was divided into three phases, an early, an intermediate and a late developmental stage. At every time within metamorphosis PTX injected animals show a higher reflex responsiveness as compared to non-injected and saline-injected animals. White lines represent median and black boxes the 25 and 75 percentile for PTX, C1 , C2 Mann-Whitney U-Test ** indicate $p < 0.01$.

development. Consequently, PTX injections can be used to determine whether increased overall neuronal excitability affects dendritic structure of identified motoneurons in the CNS. Representative examples of the dendritic structure of the adult MN5 from control and from PTX injected animals are depicted in figure 2. Projection views of all confocal optical sections into one image plane are shown side by side for a representative control injected (Fig 2A) and a representative PTX injected (Fig 2B) animal. Note that injections were conducted at pupal stage P2 (see methods). Geometric reconstructions of dendritic architecture from 3 different views are depicted for the control motoneuron shown in A (Figs 2C, E, G) and for the PTX subjected motoneuron (Figs 2D, F, H). To allow a visual comparison of the constancy of dendritic shape under control conditions, geometric reconstructions of MN5 from 3 different animals are shown in figures 2I1 to 2I3. To further demonstrate visually that overall dendritic shape remains unaltered in animals with increased excitability, figures 2I4 and 2I5 show two examples of MN5 from PTX injected animals. In all control and in all manipulated animals the overall shape of MN5 remains unchanged. The neuropil area occupied by the dendritic tree of MN5 is always approximately 400-450 µm wide, approximately 400 µm long and approximately 80 µm deep. The mean maximum dendritic path length is 370 ± 49 µm in the control dendritic trees and 358 ± 14 µm in MN5 from PTX injected animals. These data demonstrate that overall targeting and spatial restriction of dendrites within the neuropil are not affected by increased excitability. By contrast, careful visual inspection of the image stacks suggests an increase in the overall density of dendrites within the neuropil area occupied by MN5. Therefore, the data are subjected to quantitative morphometric analysis (Fig 3).

Increased excitability throughout postembryonic development increases total dendritic length (TDL) by 58 % (Fig 3A, control 37798 ± 187 µm; PTX injected 59651 ± 3104 µm). Accordingly, PTX injections cause a significant increase of MN5's dendritic surface of about 53 % (Fig 3B, from 120365 ± 27203 μm^2 to 184897 ± 17401 μm^2. The mean radius of all dendritic segments shows no significant difference between control (0.45 ± 0.1µm) and PTX injected animals (0.46 ± 0.05 µm; Fig. 3C). However, this analysis averages over all dendrites, independently of how thick they are, and is thus dominated by dendrite thicknesses that occur in large numbers within the dendritic tree. Breaking down the analysis by dendrite order may reveal specific effects of excitability on dendritic diameters (see below). The strong increase in TDL as observed in PTX

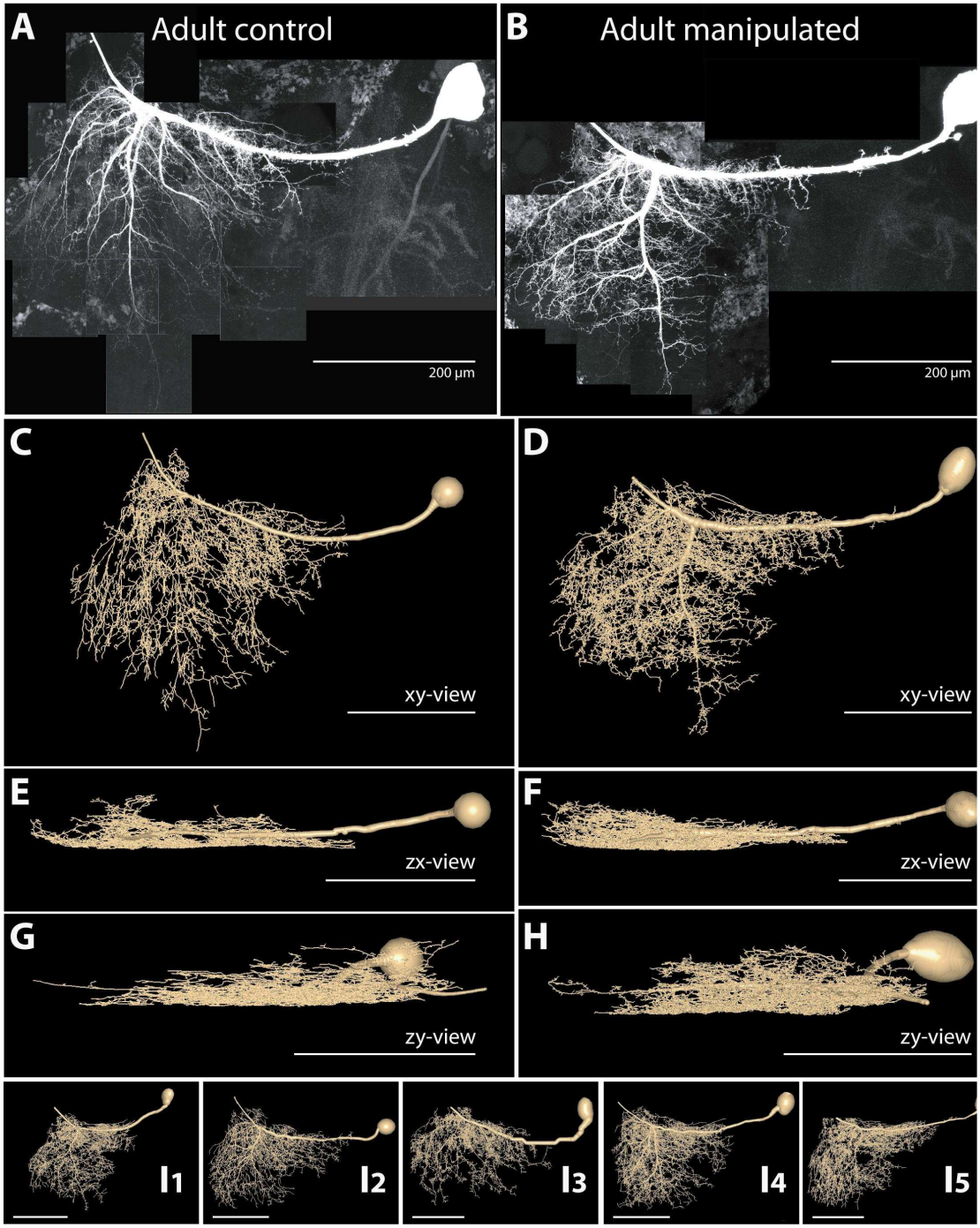
A
Adult control
200 µm
B
Adult manipulated
200 µm
C
xy-view
D
xy-view
E
zx-view
F
zx-view
G
zy-view
H
zy-view
l1
l2
l3
l4
l5

Figure 2. *Morphometric comparison of control and picrotoxin manipulated adult MN5*
Representative confocal images of control (A) and picrotoxin injected adult (B) MN5. Both images are projections views of all optical sections into one focal plane to visualize all central projections in one overview image. The cell body (cb) is located contralateral to the axon, and both are connected by a primary neurite which also gives rise to all major dendritic branches. Representative images of 3-dimensional reconstructions are depicted in xy-view in (C) for the control MN5 and in (D) for the picrotoxin injected adult MN5. Zx- orientations are shown in (E) for control and (F) for PTX injected MN5 reconstructions and in zy-view in (G) for the control and in (H) for PTX injected animals. To allow a visual assessment of variability further 3-dimensional reconstructions are shown for control MN5 (I1- I3) and PTX manipulated MN5 (I4- I5).

injected animals (Fig 3A) is caused by extra branch addition. The total number of branches is significantly increased in PTX injected animals (Fig 3D), whereas the mean length of the individual dendritic branches is even decreased as compared to controls (Fig 3E). This demonstrates that hyper-excitability causes MN5 dendrites to show less lengths growth before forming new branches and that branches are added at a much higher frequency.

To test for potential effects of altered excitability during postembryonic development on specific parts of the dendritic tree, two types of analysis were conducted. First, branch order analysis was used to test whether morphometric parameters were affected in specific parts of the dendritic tree structure only (Fig 4). Second, Sholl analysis was conducted to test whether effects on metric parameters like dendritic lengths or diameters were spatially restricted (Fig 5). For branch order analysis, a first order branch is defined as any dendrite branching off the primary neurite, which connects the cell body and the axon in MN5 (Libersat and Duch, 2004; Fig 4A). A second order branch is defined as any dendrite branching off a first order branch, and any dendrite branching off an n-order dendrite is defined as n + 1 order dendrite (Fig 4A). The spike generating zone is located close to the axo-dendritic-junction (Fig 4A ADJ; Duch, unpublished data). Analyzing the total number of dendrites as a function of the branch order reveals that hyper-excitability as induced by PTX injections causes significant overgrowth of high order branches (Fig 4B). MN5 from both groups, PTX injected and control injected animals, show similar numbers of dendrites in all branch orders between 1 and 30, indicating that early dendritic branching and the formation of all major dendrites is not affected by increased excitability. In MN5 from control animals the number of dendrites in branch orders higher that 30 decreases steeply with any further increase in branch order (Fig 4B), and the highest branch orders observed in

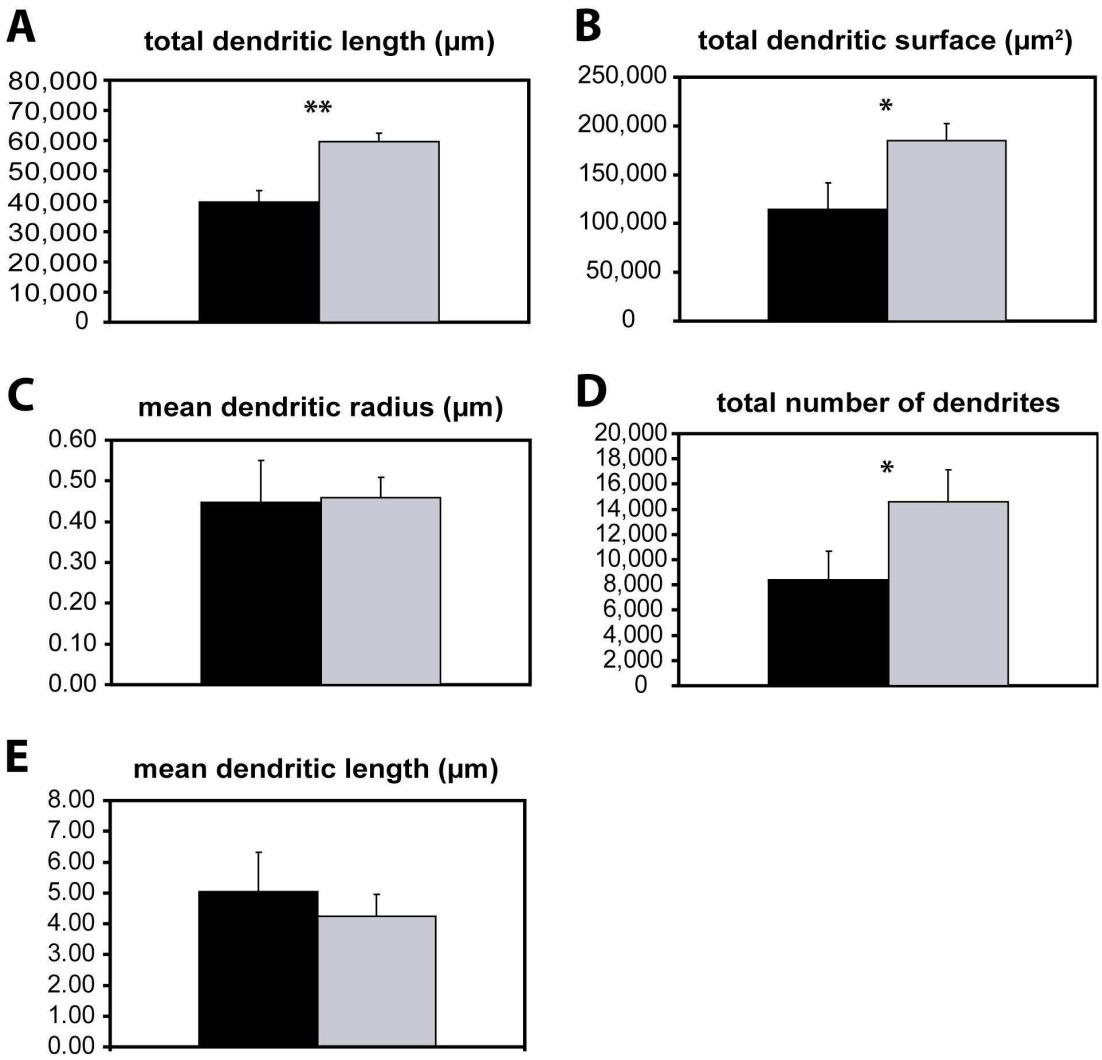

Figure 3. *Quantitative morphometric comparison of control and picrotoxin manipulated adult MN5*

Quantitative morphometric parameters as averaged from 4 representative control (black bars) and 3 representative PTX manipulated adult (grey bars) reconstructions. Total dendritic length (A) and total dendritic surface (B) are significantly increased in the manipulated adult MN5 . Mean dendritic radius (C) remains unchanged between control and manipulated animals. Total number of dendrites (D) is significantly increased. Mean dendritic length is reduced by PTX manipulation (E) but this difference is not statistically significant. Statistical significance was tested with unpaired student's t-test, ** indicate $p < 0.01$; * indicate $p < 0.05$.

controls range between 65 and 70 (69 ± 17). By contrast, in MN5 from PTX injected animals the number of branches in orders between 30 and 70 does not decrease with increasing branch order but stays relatively constant at approximately 150 dendrites in all branch orders between 30 and 60 (Fig 4B). This results in the addition of many high order branches so that the maximum branch orders in MN5 from PTX injected animals range from 85 to 100 (93 ± 13; Fig 4B). These data demonstrate that hyper-excitability

counteracts a decrease in new dendritic branch addition at branch orders higher than 30 as occurring during normal development.

Averaging the mean denritic radius over all dendrites does not reveal any differences between control and PTX injected animals (Fig 3C). However, analyzing mean dendritic radius as a function of branch order reveals that dendritic diameters are increased by approximately 30 % in all branch orders between 10 and 50 (Fig 4C). Higher order dendrites show no differences in radius between control and PTX injected animals (Fig 4C). Consequently, the basic scaffold of the dendritic tree (all major branches within the first 10 orders) is unaffected, but a massive increase in diameter occurs under conditions of hyper-excitability in all branch orders between 10 and 50. Furthermore, the diameters of high order branches (> order 50) located at the perimeter of the dendritic field are not affected by hyper-excitablity. Finally, radius is altered mostly in dendrites which exist in control and in PTX injected animals, whereas most newly added high order branches, which exist only in PTX injected animals, show the same mean radius as typical for their branch order in control animals (Figs 4B, C). As shown in figure 3E the mean length of the individual dendritic branches (MDL) is decreased in PTX injected animals. Branch order analysis demonstrates that this decrease is caused by a decrease in the length of branches in all orders below 45 but not in higher branch orders (Fig 4D). In summary, the dendritic trees of MN5 from PTX injected animals show increased numbers of high order branches, increased lengths of all individual branches in all orders below 45, and an increased diameter in all branch orders between 10 and 50.

Sholl analysis (Sholl, 1953) is a topological measurement that analyses the spatial distribution of dendritic trees. Concentric spheres (Sholl spheres) of equal diameters are created around a point of origin. Geometric parameters are then calculated within each sphere to allow comparison between different spatial distances from the point of origin. In this study, the entire length of the primary neurite that houses dendritic branches was defined as the origin of the dendritic tree, and is collapsed into one point in space mathematically (Fig 5A, see green outline). Consecutive three dimensional concentric spheres of 40 µm radius were placed around this origin of the dendritic tree (Fig 5A, white circles). To visualize all dendrites belonging to specific Sholl spheres they are depicted in different colors (blue, Sholl sphere 40 to 80; red, 120 to 160; green, 240 to 280; purple, 360 to 400µm) for a control MN5 (Fig 5B) and a reconstruction from a PTX injected animal (Fig 5C). Hyper-excitability caused an increase in dendritic length

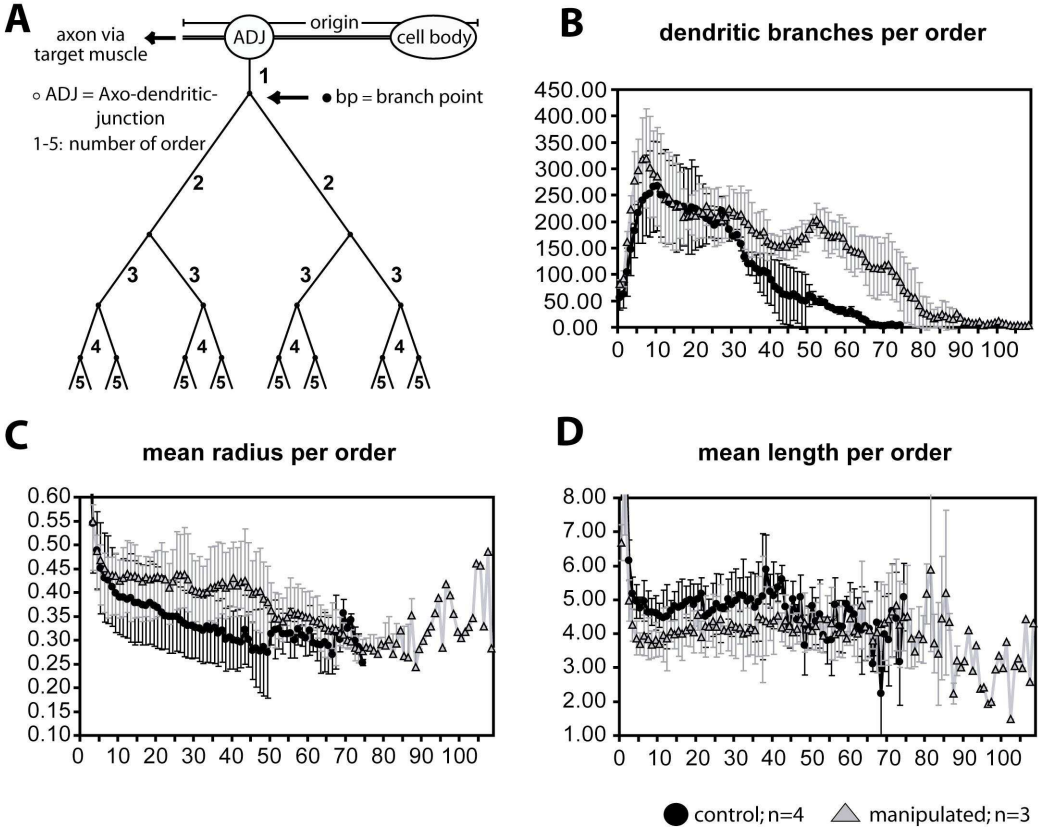

Figure 4. *Analysis of the control and manipulated dendritic tree of MN5 as a function of branch order*

(A) For branch order analysis the entire length of the primary neurite that connects the axon and the cell body and houses dendritic branches is regarded as the origin of the dendritic tree, and it is virtually collapsed into one point in space (see methods). All dendritic branches originating from the primary neurite are defined as 1st order braches, eliminating the link segments (0 order branches) between cell body and axon, and therefore collapsing the reconstruction onto one virtual origin. Every 2nd order branch branches off a 1st order branch and every following branch is a n + 1 order branch. (B) Branch order analysis shows that the number of dendrites of the manipulated MN5 is higher in the branch orders 5 to 10 and in all higher orders larger than 30 as compared to the control MN5. In the manipulated MN5 mean dendritic radius (C) is higher in all branch orders from 10 to 50 as compared to the control MN5, whereas mean dendritic length (D) is decreased in the manipulated MN5 in the branch orders up to 45.

in every Sholl sphere except the one that encompasses the first 40 µm around the primary neurite (Fig 5D). Most significant increases in dendritic length are observed in the higher Sholl spheres between 280 and 360 µm distance form the origin, which

represents the areas where many high-order dendrites in PTX injected animals. Statistical significant increases in dendritic length are marked with an asterisk (compared are mean values; ANOVA p=0.003, post-hoc Duncan-Test ** $p < 0.01$ and * $p < 0.05$). Accordingly, dendritic surface is increased significantly throughout almost all Sholl spheres (Fig 5E; ANOVA p=0.007, post-hoc Duncan-Test ** $p < 0.01$ and * $p < 0.05$). However, the increase in surface area in the distal part of the dendritic tree is less significant (Fig 5E) than the increase in dendritic length (Fig 5D) mainly because high order dendrites have a small diameter, so that increases in length do not cause large differences in total surface. The mean length of the individual dendritic branches showed no statistical significant difference in any Sholl sphere between controls and manipulated animals (Fig. 5F; ANOVA, $p = 0.31$). This is in agreement with the results from branch order analysis, where mean dendritic length is slightly longer through the branch orders in control animals, but the differences are not statistically significant (Fig 4D). Mean dendritic radius is increased in intermediate Sholl spheres in PTX injected animals (Fig 5G), but these differences are not statistically significant (ANOVA, $p = 0.39$). However, increased radii in Sholl spheres between 80 to 280 µm sholl spheres reflects the results from branch order analysis showing increased radii in the branching orders 10 to 50 (Fig 4C).

In summary, these morphometric data clearly demonstrate that hyper-excitability as induced by systemic injections of PTX during postembryonic dendritic growth clearly cause overgrowth of the dendritic tree, mainly by the addition of many high order branches. In addition the radii of the individual dendritic branches are slightly increased in all the branch orders 10 to 50. Consequently, the dendritic tree comprises more surface area and thus clearly more space for putative synaptic contacts. But is dendritic overgrowth accompanied by an increase in synaptic input? And in the specific case of inducing hyper-excitability by blocking chloride channels associated with GABA receptors, is the number of GAGAergic inputs onto the dendritic tree of MN5 increased?

We have recently demonstrated that the number of GABAergic input synapses impinging on the dendritic tree of an indentified motoneuron can be estimated by evaluating high resolution confocal laser scanning images (Schmitt et al., 2004; Evers et al., 2005; 2006; Duch and Mentel, 2004; Hohensee et al., 2007). To localize and quantify the juxtaposition of presynaptic sites to the dendritic arbor, the cell surface of the neuronal arborization is reconstructed from confocal image stacks, and the

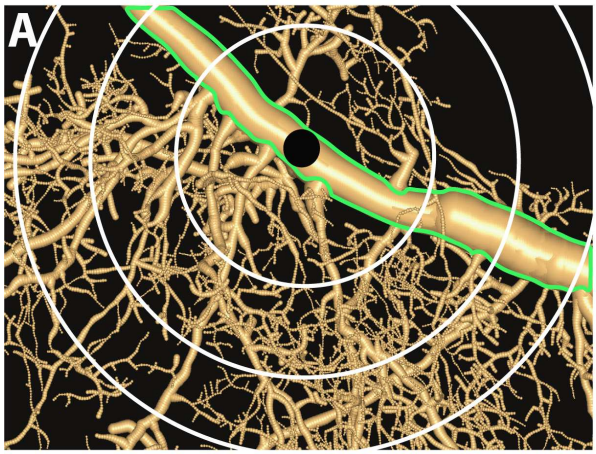
A

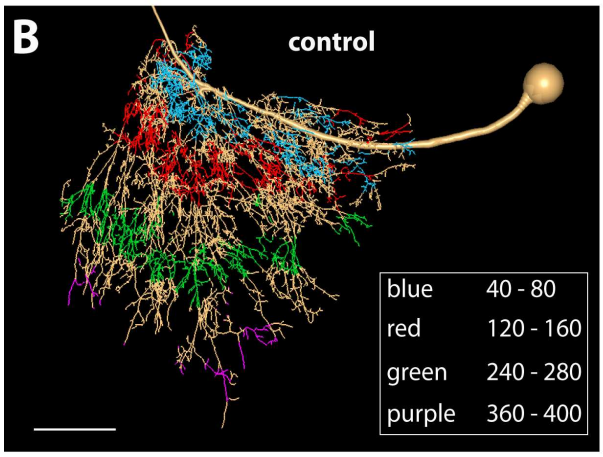
B
control
blue 40 - 80
red 120 - 160
green 240 - 280
purple 360 - 400

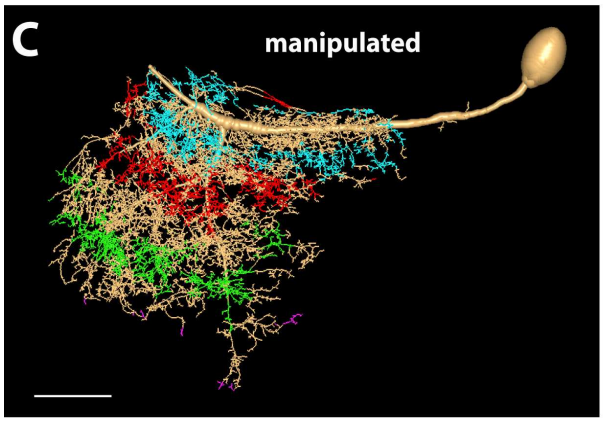
C
manipulated

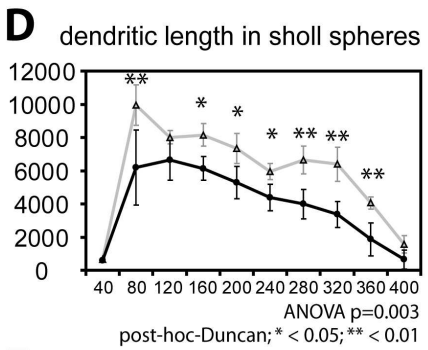
D
dendritic length in sholl spheres
12000
10000
8000
6000
4000
2000
0
40 80 120 160 200 240 280 320 360 400
ANOVA p=0.003
post-hoc-Duncan; * < 0.05; ** < 0.01

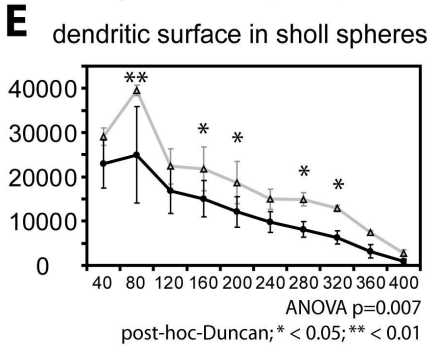
E
dendritic surface in sholl spheres
40000
30000
20000
10000
0
40 80 120 160 200 240 280 320 360 400
ANOVA p=0.007
post-hoc-Duncan; * < 0.05; ** < 0.01

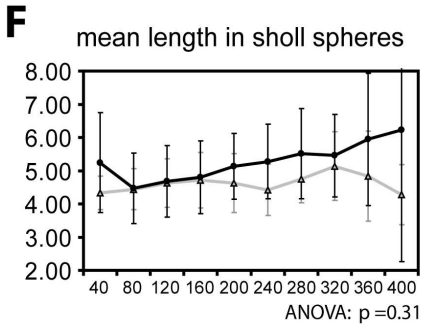
F
mean length in sholl spheres
8.00
7.00
6.00
5.00
4.00
3.00
2.00
40 80 120 160 200 240 280 320 360 400
ANOVA: p =0.31

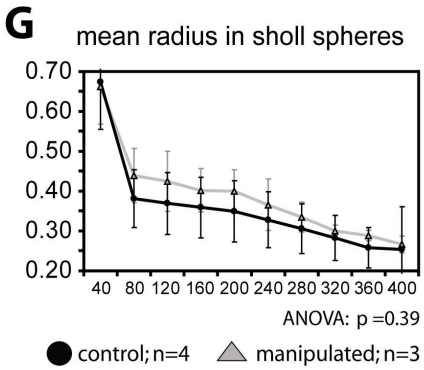
G
mean radius in sholl spheres
0.70
0.60
0.50
0.40
0.30
0.20
40 80 120 160 200 240 280 320 360 400
ANOVA: p =0.39
control; n=4
manipulated; n=3

Figure 5. *Scholl analysis of morphometric parameters*
For Sholl analysis the entire length of the primary neurite that connects the axon and the cell body and houses dendritic branches is regarded as the origin of the dendritic tree (A, see green outline, see also methods and Fig 4A), and it is virtually collapsed into one point in space (black dot). Sholl spheres are defined as consecutive concentric spheres of 40 µm radius (white circles in A) around the origin (black dot). For visualization different colors signify different Sholl spheres (blue, Sholl sphere 40 to 80; red, 120 to 160; green, 240 to 280; purple, 360 to 400µm) for the control dendritic tree (B) and in the manipulated dendritic tree of MN5 (C). (D) – (G) Shown are mean and standard deviation within a Sholl sphere plotted as a line diagram for each sphere for the control MN5 (black line and dots) and for the manipulated MN5 (grey line and triangles). Mean dendritic length (D) and mean dendritic surface (E) per sphere are increased in manipulated animals compared to control. (F) shows the mean dendritic length per sphere demonstrating a decrease in segment length for manipulated animals in nearly all spheres although not significantly different. Mean radius in manipulated animals is increased (G) in every sphere without the first as has been demonstrated in branch order analysis. Significant differences between different Sholl spheres are highlighted by asterisks (ANOVA, Duncans post-hoc test, * indicate $p < 0.05$; ** indicate $p < 0.01$)

colocalization probability of immunolabeled GABA and synapsin-I profiles is calculated for each surface element within a 300nm distance. Using triple labels for MN5, GABA and synapsin-I we charted the distribution pattern of GABAergic input synapses onto the dendritic tree of MN5. As an example, in figure 6A1 a single reconstructed dendritic branch is superimposed on an optical section from a whole-mount immunostained neuropil against GABA (green). Every surface element of the dendrite reconstruction is color coded for the mean GABA-immunolabel staining intensity within 300 nm distance, with warmer colors indicating higher co-localization. In figure 6A2 the corresponding optical section of the anti-synapsin I immunolabel (blue) is shown accordingly. To highlight synaptic terminals which contain GABA, we calculated a correlation coefficient of both, the anti-GABA- and anti-synapsin I image data. We extracted the average correlation value within 300nm distance to the neuronal surface in order to restrict the analysis to GABAergic synapses only which are in juxtaposition to the dendritic surface of MN5 (Fig 6A3). Applying this procedure to all optical sections produced a complete map for the distribution of putative GABAergic input synapses onto the entire dendritic tree for control injected (Fig 6B1) and for PTX injected animals (Fig 6B2). We have previously demonstrated that relative synapse numbers detected with this method correlate with electrophysiological analysis of the numbers and amplitudes of postsynaptic potentials (Duch and Mentel, 2004), and correlative electron- and confocal microscopy study further demonstrates the validity of this procedure for estimating the number of putative GABAergic inputs (Hohensee et al., 2007). In control animals, about 7 percent of the dendritic surface of MN5 receives

putative GABAergic input (Fig 6C, black bar). By contrast, in PTX injected animals only about 2 percent of the dendritic surface is contacted by GABAergic terminals (Fig 6C, grey bar). Consequently, the dendritic surface area contacted by GABAergic terminals in relation to the total dendritic surface area is more than 3 times smaller in PTX than in control injected animals. Even when taking into consideration that total dendritic surface is nearly doubled in PTX injected animals (Fig 2B), these data demonstrate that the net number of GABAergic terminals contracting MN5 is decreased by PTX injection. Consequently, blocking GABA mediated inhibition during postembryonic development causes dendritic overgrowth but a decrease in GABAergic input.

However, in a recent study we have demonstrated that GABAergic inputs are not distributed randomly throughout the dendritic tree on MN5. By contrast, after normalizing the surface are of MN5 contacted by GABAergic terminals by dividing it by total surface area within each Sholl sphere, it was apparent that GABAergic inputs occur with a much higher likelihood in high Sholl spheres at the perimeter of the dendritic tree than in lower Sholl spheres close to the origin of the tree. Interestingly, such synapse distribution rules occur in a stage specific manner during postembryonic development and can be related to behavioral function (Meseke et al., unpublished). Opening of chloride channels as mediated by $GABA_A$ receptor activation is not required for the development of such adult specific synapse distribution patterns, because PTX injected animals show similar distribution patterns of GABAergic inputs through the Sholl as compared to controls (Fig 6D1). As the total number of GABAergic terminals contacting MN5 is lower but the total surface area is larger than in controls, PTX injected animals show less relative surface contacted by GABAergic terminals in every single Sholl sphere (Fig 6D1). However, the fact that higher Sholl spheres receive significantly more relative GABAergic input per area surface holds for control and for PTX injected animals (Fig 6D1). The radii of Sholl spheres can be calculated using linear distances from the point of origin (Fig 6D2, red arrow 1, air distance). However, the run of dendrites is rarely straight, but curved in most cases, and electrical signal attenuate as a function of distance along the actual run of dendrites. Therefore, using the distance along the run of the dendrites (Fig 6E2, red arrow 2, tree distance) is a more functional measure for defining the radii of Sholl spheres. Using this procedure also demonstrates a clear preference for GABAergic terminals to contact the dendritic tree of

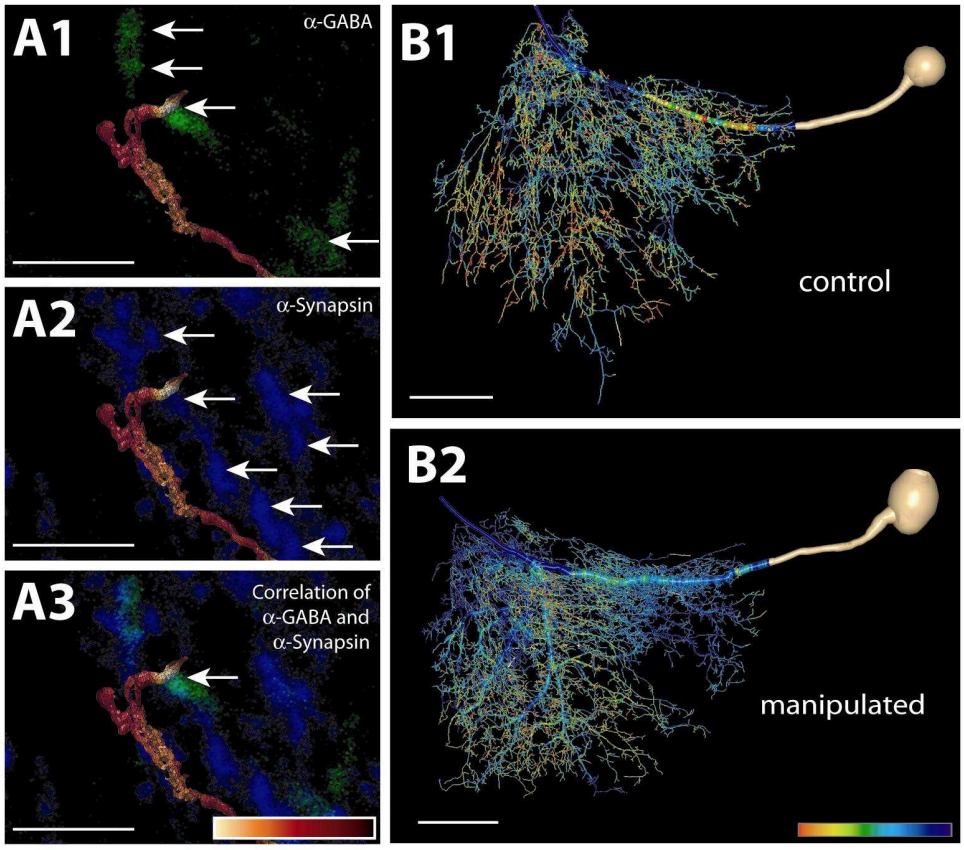
A1
α-GABA
A2
α-Synapsin
A3
Correlation of
α-GABA and
α-Synapsin
B1
control
B2
manipulated

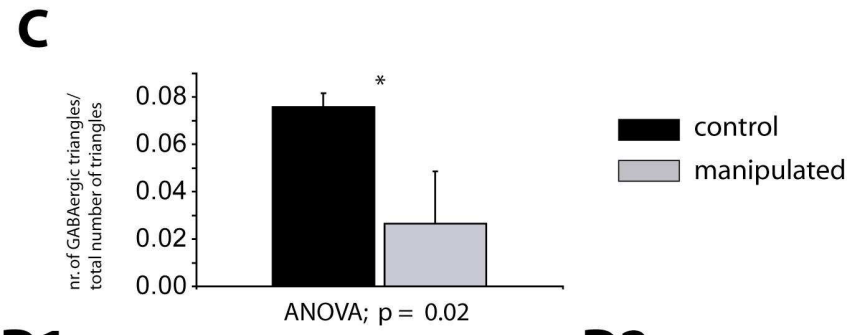
C
nr. of GABAergic triangles/
total number of triangles
0.08
0.06
0.04
0.02
0.00
*
control
manipulated
ANOVA; p = 0.02

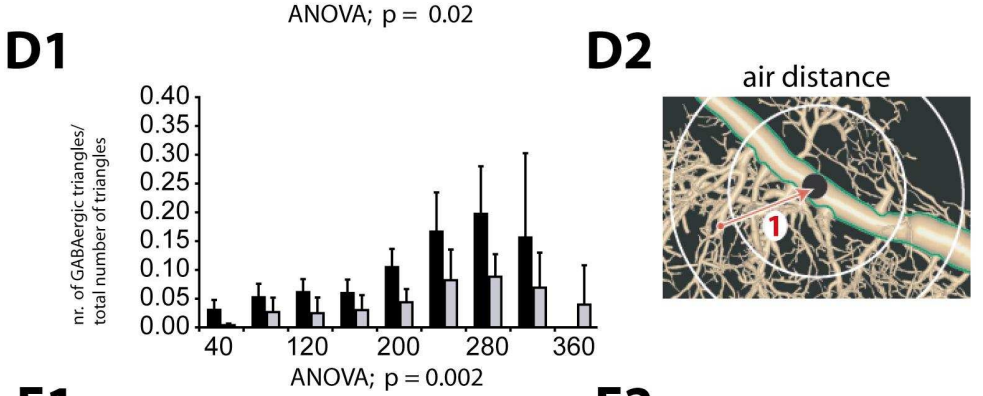
D1
nr. of GABAergic triangles/
total number of triangles
0.40
0.35
0.30
0.25
0.20
0.15
0.10
0.05
0.00
40
120
200
280
360
ANOVA; p = 0.002
D2
air distance
1

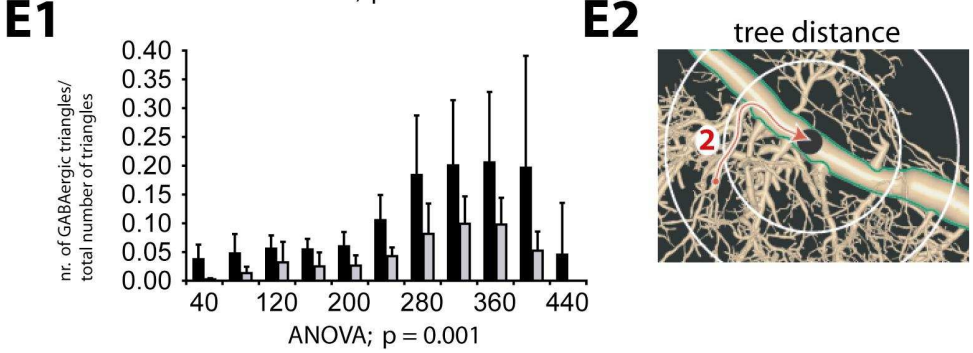
E1
nr. of GABAergic triangles/
total number of triangles
0.40
0.35
0.30
0.25
0.20
0.15
0.10
0.05
0.00
40
120
200
280
360
440
ANOVA; p = 0.001
E2
tree distance
2

Figure 6. *Mapping of putative GABAergic inputs onto the dendritic surface of MN5*
The surface of MN5 is reconstructed from confocal image stacks, and the co-localization probability of GABA and synapsin-I is calculated for each surface element within a 300nm distance. The method is exemplified in (A) with a selective enlargement of one optical section through a dendritic arbor. First, the surface reconstruction is superimposed on a single optical section of anti-GABA immunostaining (green, A1). Each element of the surface reconstruction is color coded for the mean GABA-immunostaining intensity within 300 nm distance, with whitish colors (glow-over mode) indicating higher anti-GABA staining intensity. The same procedure is shown for anti-synapsin-I immunostaining from the same optical section (A2). The correlation of both mappings is depicted in (A3). This method is applied for the entire dendritic tree of the control (B1, black bar) and the manipulated MN5 (B2, grey bar), whereby warmer colors indicate a higher anti-GABA staining intensity. (C1) depicts the normalized amount of GABAergic inputs (GABAergic surface/total dendritic surface) within the whole dendritic tree of the control (black bar) and the manipulated MN5 (grey bar). In (D1) the Sholl spheres are defined as the linear distance to the dendrite's origin (D2, air distance, see methods), and in (E1) Sholl spheres are defined using distance along the midline (E2, tree distance) in 3 dimensional space. For normalization the surface area in contact to a putative GABAergic input synapse is divided by the total surface area within each Sholl sphere and plotted as a bar diagram for each sphere (D1, E1) for the control MN5 (black bars) and for the manipulated MN5 (grey bars). Both types of analyses show non random, predominantly in the outer perimeter of the dendritic field located putative GABAergic synapse distribution for control and manipulated animals. However, manipulated animals show a reduced amount of putative GABAergic synapses within every sphere. Significant differences between groups (control/ manipulated) are indicated by asterisks (ANOVA, * indicate $p < 0.05$). Scale is 5 µm (A) and 100µm (B).

MN5 in higher Sholl spheres (Fig 6E1). Therefore, sub-dendritic site specific targeting of putative GABAergic synapse does not rely on the activation of chloride channels.

In summary PTX injections during postembryonic development influence the geometry of the dendritic tree of MN5 as well as the density of putative GABAergic inputs, but not the distribution of GABAergic inputs through the dendritic tree. One obvious question is whether the observed morphological changes and the decreased inhibitory input do alter behavioral output? As a first step towards answering this question we simply assayed whether adult animals from different experimental groups showed normal likelihoods to engage into stationary flight motor behavior. Figure 7A shows that 87.5 percent of all animals that were not injected at all (n = 20) responded to a wind stimulus with stationary flight when restrained to a stick (see methods). Control injections at pupal stage 2 with saline did not reduce the percentage of flyers (n = 25; Fig 7A). However, PTX injections at pupal stage P2 reduced the percentage of flyers to 75 percent (n = 45; Fig 7A). This shows that dendritic overgrowth or a reduction in the number of GABAergic synapses, or a combination of both actually reduces the likelihood to take-off. To control whether all PTX injected animals were in principle able to take-off, we forced take-off by systemic injections of the octopamine agonist

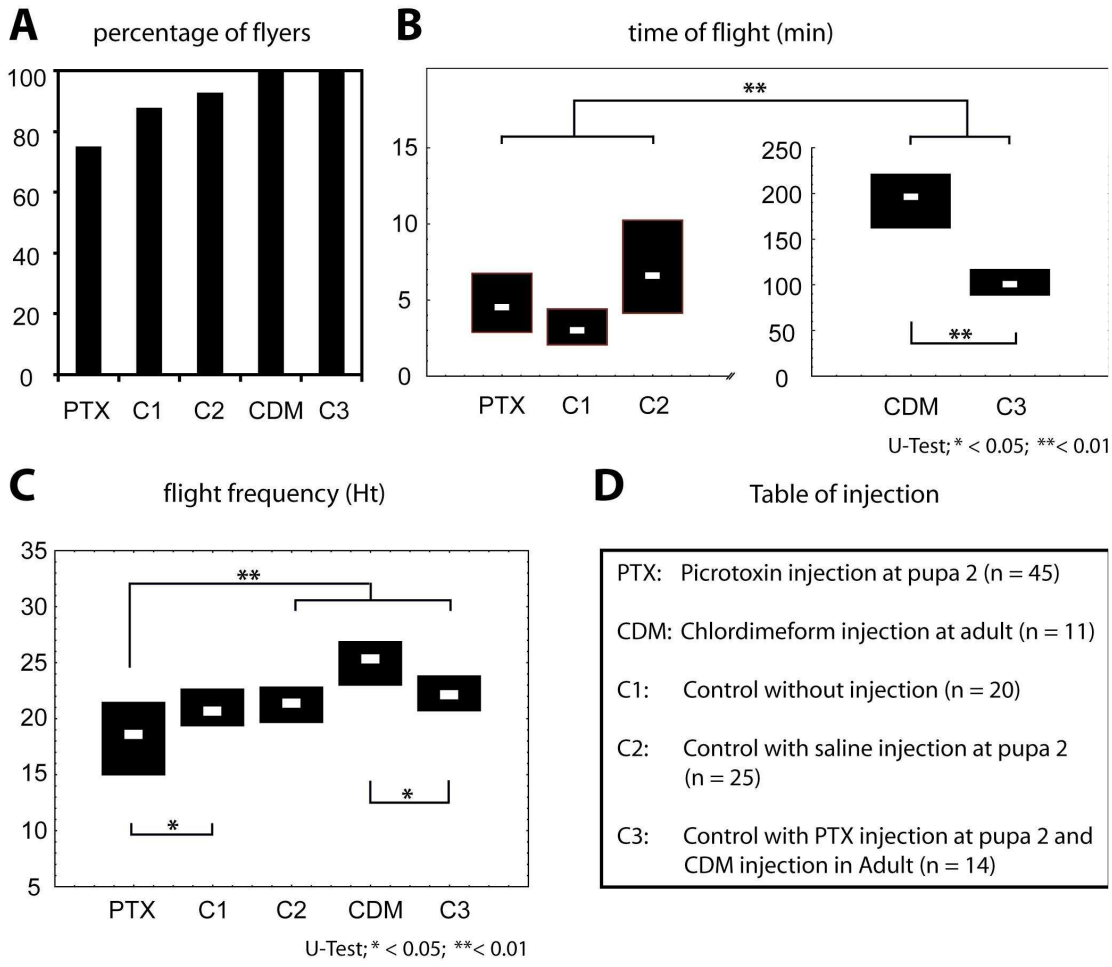

Figure 7. *Comparison of stationary flight ability of control and PTX injected adult animals* (A) depicts the percentage of flying animals in dependence to drug treatment. For a better overview the different methods of treatment are listed in (D) as well as the number of animals per group investigated. (B) shows the time of flight measured in minutes for the differently treated groups. Note the different scale on y-axis within (B) for CDM injected animals (right panel). (C) shows the wing beat frequency during stationary flight measured in heart (ht) for the differently treated groups. White lines indicate median and black boxes 25 and 75 percentile. Significant differences are marked with asterisks (Kruskall-Wallis ANOVA, Mann-Whitney U-Test * indicate $p < 0.05$; ** indicate $p < 0.01$).

chlordimeform (CDM, see methods) into adult moths. CDM injections into control animals yielded 100 percent flyers (n = 11, Fig 7A). Similarly, CDM injections into animals which were injected with PTX at pupal stage P2 yielded 100 percent flyers (n = 14 , Fig 7A), demonstrating that the structural alterations caused by PTX injections did not hinder the ability to take-off. Total in flight duration was unaltered when comparing non-injected controls saline injected controls and PTX injected animals (Fig 7B),

demonstrating that structural changes as occurring upon PTX injections during early pupal life do not affect the duration of flight as a response to consecutive wind stimuli (see methods). However, if flight was forced pharmacologically by CMD injections, flight duration was significantly increased in these animals but only half as much increased in animals that had been injected with PTX at stage P2 (Fig 7B). This demonstrates that maximum motor endurance was significantly decreased in animals that had seen PTX injections during early pupal life. Wing beat frequencies as occurring during stationary flight are significantly different on the one hand between PTX injected and on the other hand no-injected and control injected animals (Fig 7C). However, CDM injection increases wing beat frequencies significantly in control animals but not in previously PTX injected animals (Fig 7C). This further suggests that maximum performance might be impaired in animals with PTX induced structural alterations in the nervous system, i.e. motoneuron dendritic overgrowth and a reduction in putative GABAergic inputs to motoneurons.

3.5 Discussion

This study demonstrates that pharmacological blockade of chloride channels by systemic injections of PTX induce increased excitability throughout adult development. This, in turn, causes increased branching of high order dendrites, a decrease in the density of GABAergic inputs impinging on the dendritic tree, and it affects motor performance of the adult. In various systems, multiple roles for $GABA_A$ receptor activated chloride channels have been reported during different phases of development, such as promoting synaptogenesis, sculpting temporal and spatial aspects of synaptic integration and controlling excitation / inhibition ratios (Ben-Ari, 2002; Akerman and Cline, 2007). However, during vertebrate brain development $GABA_A$ receptor signalling changes from being excitatory to being inhibitory because the resting intracellular chloride concentration is controlled by developmental and activity-dependent regulation of chloride transporters (Fiumelli and Woodin, 2007). In addition $GABA_A$ receptor conductance becomes increasingly faster during development. By contrast, by using insect metamorphosis as a model the analysis is most likely reduced to and focused on $GABA_A$ receptor mediated inhibition with a constant conductance time throughout metamorphosis, because no developmental regulation of the chloride resting potential or of $GABA_A$ receptor conductance has been found during metamorphosis.

3.5.1 Increased excitability causes dendritic overgrowth

The most prominent morphological alteration caused by PTX injections is overgrowth of the dendritic tree, due to an increased branching rate. Accordingly, in the visual system, enhanced activity driven by light promotes dendritic growth of tectal cells in a NMDA receptor dependent manner (Sin et al., 2002), in cultured olfactory bulb neurons blockade of $GABA_A$ channels increases dendritic branching (Matsutani and Yamamoto, 1998), and in cultured rat hippocampal neurons PTX-induced increases in neural activity increase dendritic spine density (Papa and Segal, 1996). Despite a marked increase in the number of dendritic branches, the overall morphology of the dendritic tree and its perimeter remain unaltered. This agrees with findings on altered central circuit excitability during Drosophila embryonic development, where genetic knock-down of sensory synaptic transmission does not impair basic locomotor circuit assembly but alters the actual patterns of locomotion during later stages (Suster and Bate, 2002). Similarly, imposed changes of motoneuron intrinsic activity during late larval life of Manduca does not stop steroid induced dendritic regression, but alters the number of high order dendritic branches (Duch and Mentel, 2004).

However, the effects of neural activity on developing dendrites vary between different species, different types of neurons and different developmental times (Libersat and Duch, 2004; Lohmann and Wong, 2005). In general, one has to distinguish between experience-dependent activity transmitted synaptically by afferent neurons (Zhang et al., 2000), and endogenous activity in developing neurons and circuits that occurs independently of sensory feedback (Weliky and Katz, 1999; Feller, 1999). Furthermore, within individual neurons action potential mediated depolarisations may lead to global increases in intracellular calcium concentrations that control dendritic properties by regulating transcription (West et al., 2002), whereas detailed branching patterns of dendritic arbors may be regulated by local calcium increases triggered by strictly local synaptic input (Lohmann et al., 2002; Niell at al., 2004). At current the mechanisms by which systemic PTX injections mediate increased branching remain speculative, because it is not clear whether global blockade of chloride channels affects mainly local synaptic transmission, or whether the resulting intrinsic spiking activity of the neurons under investigation is altered, or whether overall spiking level and patterns of the entire developing circuitry is altered.

3.5.2 Increased excitability affects inhibitory input synapse density and dendritic diameter

The dendritic tree of MN5 from PTX injected animals comprises more surface area and thus clearly more space for putative synaptic contacts. However, following PTX injections we find a significantly reduced density of putative GABAergic synapses impinging on the dendritic tree of MN5, even before normalizing to total dendritic surface. This clearly indicates a net loss of GABAergic inputs into the dendritic tree of MN5. This seems counter-intuitive, because numerous studies have demonstrated the existence of compensatory homeostatic control mechanisms opposing manipulations of synaptic activity or membrane excitability during neural circuit development (Spitzer, 1999; Turrigiano, 1999; Marder and Prinz, 2002, Marder and Goaillard, 2006). By contrast, we find a reduced number of inhibitory terminals impinging on a dendritic tree in response to hyper-excitability. This seems to oppose the idea of synaptic homeostatic plasticity because the system appears to react in the same direction to what has created the disturbance in the first place. However, since we simply counted putative GABAergic terminals we can not exclude scaling of the existing synaptic contacts. Although most of what is known about synaptic homeostatic mechanisms comes from studies on excitatory synapses (Turrigiano et al., 1998; 2000), recent work has also revealed bidirectional scaling of $GABA_A$ receptor mediated inhibition (Modi, 2005). Synaptic scaling can be achieved postsynaptically by changing the numbers of GABA receptors (Kilman et al., 2002) and presynaptically by altering the number of vesicular GABA transporters (De Gois et al., 2005). Our study does not account for any of these two mechanisms, and thus, we can not conclude whether or not synaptic scaling takes place as a homeostatic response to reduced $GABA_A$ receptor mediated inhibition. Nevertheless, we can state that PTX injections can not be fully compensated for because the animals are clearly hyper-excitable throughout postembryonic development following the time point of injection. Furthermore, the number of GABAergic terminals impinging on the dendritic tree of MN5 is strongly reduced upon chloride channel block, which clearly reduced the investment into large numbers of GABAergic terminals which are not functionally effective. Reducing the number of synapses in a circuit significantly reduces the energy costs per spike, and spikes expenses are high so that they require the brain to use representational codes that rely on the activity of a limited number of neurons (Lennie, 2003).

However, we found a morphological change which most likely opposes pharmacologically induced hyper-excitability. Dendritic diameters are increased by approximately 30 % in dendrites of the orders 10 to 50. Increasing dendritic radii requires a higher investment into new membrane, so it opposes housekeeping considerations. By contrast, propagation of electric signals within a dendritic tree depends on dendritic morphology (Gwilliam and Burrows, 1980; Koch and Segev, 2000; Vetter et al., 2001) and an increase in diameter reduces axoplasmatic resistance and enhances PSP propagation distance. This could be a possible mechanism compensating for reduced $GABA_A$ receptor mediated inhibition. Therefore, it might be that dendritic architecture has to be considered as regulatory factor involved in the delicate balance of homeostatic plasticity.

3.5.3 Sub-dendritic targeting of inhibitory synapses does not depend on GABAA receptor activity

We have recently demonstrated that putative GABAergic input synapses are not randomly distributed throughout the dendritic tree of MN5. By contrast sub-dendritic synapse targeting causes a significantly higher density of GABAergic inputs in distal dendrites towards the perimeter of the dendritic field in proximal dendrites close to the tree origin. Furthermore, sub-dendritic synapse targeting is not a function of neuropil structure but must rely on specific sub-dendritic recognition mechanisms (Meseke et al., unpublished). This study clearly demonstrates that sub-dendritic targeting of GABAergic synapses occurs independent of the activation of $GABA_A$ receptors. Therefore, different parts of the dendritic tree must contain specific molecular addresses for precise sub-cellular target recognition. Experience or activity dependent site specific pruning following a genetically determined axon guidance process (Tessier-Lavigne and Goodman, 1996) can be ruled out. Similarly, targeting of two different types of GABAergic inputs along the perisomatic and dendritic domains of pyramidal neurons in visual cortex (Freund and Buzsaki, 1996) does not rely on experience dependent thalamic input (Di Cristo et al., 2004). Molecular encoding of a proximal to distal axis within neurons is further supported by sub-neuronal targeting of Kv 2.1 potassium channels (Lim et al., 2000), and AMPA receptors in pyramidal neurons (Magee and Cook, 2000; Andrasfalvy and Magee, 2001).

3.5.4 Functional consequences of PTX induced overgrowth and decreased GABAergic input synapse density

The behavioral function of MN5 in the adult moth is to produce part of the flight motor output (Casadey and Camhi, 1976; Duch et al., 2000). To ensure adequate contractions of the DLM flight muscle MN5 must fire one action potential at the correct time point within each wing-beat cycle. At a wing beat frequency of approximately 25 Hz and massive sensory feedback during flight, this means that multiple synaptic inputs must be computed by the dendritic tree of MN5 to generate spikes with a high temporal precision, probably within a time window of few milliseconds. Blocking $GABA_A$ receptor mediated chloride current during postembryonic circuit development does not impair flight motor output, but endurance and maximum wing beat frequencies are reduced. This suggests that hyperpolarizing GABAergic input might serve to narrow temporal synaptic integration windows during circuit refinement and thereby decrease maximum flight performance. This is in line with findings in hippocampus, where developmental shifts in the induction rules for LTP depend on maturational changes in hyperpolarizing GABAergic activity (Meredith et al., 2003). Furthermore, preventing the development of hyperpolarizing GABAergic activity in cortical layer IV neurons by ablation subplate neurons in visual cortex impairs the formation of precise neural circuits underlying orientation selectivity (Kanold and Shatz, 2006). A role of $GABA_A$ mediated inhibition for circuit refinement as an evolutionary conserved principle also occurring in invertebrates is an attractive hypothesis. However, this study is lacking conclusive evidence for this hypothesis because it analyzed dendritic architecture and synapse distribution of a single motor neuron only, and not the properties of flight motor circuitry. Consequently, the observed behavioral differences after reduced $GABA_A$ mediated inhibition during postembryonic development might also be caused by the observed increase in dendritic length, or by some other features of the nervous system that were affected but not sampled.

3.6 References

Akerman CJ, Cline HT (2007) Refining the roles of GABAergic signalling during neural circuit formation. TINS 30: 382-389.

Andrasfalvy BK, Magee JC (2001) Distance-dependent increase in AMPA receptor number in the dendrites of adult hippocampal CA1 pyramidal neurons. J Neurosci 21:9151-9159.

Bate CM (1973) The mechanism of the pupal gin trap. I. Segmental gradients and the connections of the triggering sensilla. J Exp Biol 59: 95 – 107.

Bell RA, Joachim FA (1976) Techniques for rearing laboratory colonies of tobacco hornworms and pink ballworms. Ann Entomol Soc Am 69:365-373.

Ben-Ari Y (2002) Excitatory actions of GABA during development: The nature of the nurture. Nat Rev Neurosci 3:728-739.

Burkart P, Duch C (2006) Developmental changes of CaMKII localization, activity and function during postembryonic CNS remodelling in Manduca sexta. Eur J Neurosci 23(2):335-349.

Casadey GB, Camhi JM (1976) Metamorphosis of flight motoneurons in the moth, *Manduca sexta*. J Comp Physiol 112:143-158.

Cooke BM, Woolley (2005) Sexually dimorphic synaptic organization of the medial amygdala. J Neurosci. 25(46):10759-10767.

Connors BW, Regehr WG (1996) Neuronal firing: does function follow form? Curr Biol 12:1560-1562.

Consoulas C, Duch C, Bayline RJ, Levine RB (2000). Behavioral transformation during metamorphosis: remodeling of neural and motor systems. Brain Res Bull 53(5):571-583
De Gois et al. (2005) Homeostatic scaling of vesicular glutamate and GABA transporter expression in rat neocortical circuits. J Neurosci 25:7125-7133.

Di Christo G, Wu C, Chattopadhyaya B, Ango F, Knott G, Welker E, Svoboda K, Huang ZJ (2004) Subcellular domain-restricted GABAergic innervation in primary visual cortex in the absence of thalamic inputs. Nat Neuroscience 7:1184-1186.

Duch C, Levine RB (2000). Remodeling of membrane properties and dendritic architecture accompanies the postembryonic conversion of a slow into a fast motoneuron. J Neurosci 20(18):6950-6961.

Duch C, Levine RB (2002). Changes in calcium signaling during postembryonic dendritic growth in *Manduca sexta*. J Neurophysiol 87(3):1415-1425.

Duch C, Mentel T (2004) Activity affects dendritic shape and synapse elimination during steroid controlled dendritic retraction in *Manduca sexta*. J Neurosci 24(44):9826-9837.

Evers JF, Schmitt S, Sibila M, Duch C (2005) Progress in functional neuroanatomy: precise automatic geometric reconstruction of neuronal morphology from confocal image stacks. J Neurophysiol 93(4):2331-2342.

Evers JF, Münch D, Duch C (2006). Developmental relocation of presynaptic terminals along distinct types of dendritic filopodia. Dev Biol 297(1):214-227.

Fiumelli H, Woodin MA (2007) Role of activity-dependent regulation of neuronal chloride homeostasis in development. Curr Opin Neurobiol 17: 81-86.

Freund TF, Buzsáki G (1996) Interneurons of the hippocampus. Hippocampus 6(4):347-470.

Gao FB, Bogert BA (2003) Genetic control of dendritic morphogenesis in Drosophila. Trends Neurosci. 26(5):262-268.

Gwilliam GF, Burrows M (1980) Electrical characteristics of the membrane of an identified insect motorneurone. J Exp Biol 86:49-61

Häusser M, Spruston N, Stuart GJ (2000) Diversity and dynamics of dendritic signaling. Science 290(5492):739-744.

Hofer SB, Mrsic-Flogel TD, Bonhoeffer T, Hübener M (2006) Lifelong learning: ocular dominance plasticity in mouse visual cortex. Curr Opin Neurobiol 16(4):451-459.

Hohensee S, Bleiss W, Duch C (2007) Correlative electron and confocal microscopy assessment of synapse localization in the central nervous system of an insect. J Neurosci Methods [Epub ahead of print]

Kanold PO, Shatz CJ (2006) Subplate neurons regulate maturation of cortical inhibition and outcome of ocular dominance plasticity. Neuron 51:627-638.

Kapfer C, Seidl AH, Schweizer H, Grothe B (2002) Experience-dependent refinement of inhibitory inputs to auditory coincidence-detector neurons. Nat Neurosci 5(3):247-253.

Koch C, Segev I (2000). The role of single neurons in information processing. Nat Neurosci 3:1171-1177.

Kilman V, van Rossum MC, Turrigiano GG (2002) Activity deprivation reduces miniature IPSC amplitude by decreasing the number of postsynaptic $GABA_A$ receptors clustered at synapses. J Neurosci 22: 1328-1337.

Kim S, Chiba A (2004) Dendritic guidance. Trends Neurosci. 27(4):194-202.

Kinnamon SC, Klaassen LW, Kammer AE, Claassen D (1984) Octopamine and chlordimeform enhance sensory responsiveness and production of the flight motor pattern in developing and adult moths. J Neurobiol 15(4):283-293.

Landgraf M, Thor S (2006) Development and structure of motoneurons. Int Rev Neurobiol. 75:33-53.

Landgraf M, Thor S (2006) Development of Drosophila motoneurons: specification and morphology. Semin Cell Dev Biol. 17(1):3-11.

Lemon WC, Levine RB (1997A) Multisegmental motor activity in the segmentally restricted gin trap behavior in *Manduca sexta* pupae. J Comp Physiol [A] 180(6):611-9.

Lemon WC, Levine RB (1997B) Segmentally distributed metamorphic changes in neural circuits controlling abdominal bending in the hawk moth *Manduca sexta*. J Comp Physiol [A] 180(6):597-610.

Lennie P (2003) The cost of cortical computation. Curr Biol 13(6):493-497.

Levine RB, Weeks JC (1996). Cell culture approaches to understanding the actions of steroid hormones on the insect nervous system. Dev Neurosci 18:73-86.

Libersat F, Duch C (2002) Morphometric analysis of dendritic remodeling in an identified motoneuron during postembryonic development. J Comp Neurol 450(2):153-166

Libersat F, Duch C (2004) Mechanisms of dendritic maturation. Mol Neurobiol 29(3):303-320.

Lim ST, Antonucci DE, Scannevin RH, Trimmer JS (2000) A novel targeting signal for proximal clustering of the Kv2.1 K+ channel in hippocampal neurons. Neuron 25:385-397.

Lohmann C, Finski A, Bonhoeffer T (2005). Local calcium transients regulate the spontaneous motility of dendritic filopodia. Nat Neurosci 8(3):305-312

Lohmann C, Myhr KL, Wong RO (2002) Transmitter-evoked local calcium release stabilizes developing dendrites. Nature 418(6894):177-181.

Lohmann C, Wong RO (2005) Regulation of dendritic growth and plasticity by local and global calcium dynamics. Cell Calcium 37(5):403-409.

Magee JC, Cook EP (2000) Somatic EPSP amplitude is independent of synapse location in hippocampal neurons. Nat Neurosci 3:895-903.

Marder E, Prinz AA (2002). Modeling stability in neuron and network function: the role of activity in homeostasis. Bio Essays 24:1145-1154.

Marder E, Goaillard JM (2006). Variability, compensation and homeostasis in neuron and network function. Nat Rev Neurosci 7(7):563-574.

Matsutani S, Yamamoto N (1998). GABAergic neuron-to-astrocyte signaling regulates dendritic branching in coculture. J Neurobiol 37(2):251-267

Meredith RM, Floyer-Lea AM, Paulsen O (2003) Maturation of long-term potentiation induction rules in rodent hippocampus: role of GABAergic inhibition. J Neurosci 23(35):11142-11146.

Meseke M, Evers JF, Duch C (unpublished) Sub-dendritic synapse targeting and postembryonic dendritic geometry remodeling of an identified neuron subserve its changing behavioral role.

Mizrahi A, Ben-Ner E, Katz MJ, Kedem K, Glusman JG, Libersat F (2000) Comparative analysis of dendritic architecture of identified neurons using the Hausdorff distance metric. J Comp Neurol 422(3):415-428.

Modi I (2005) Aspects of the homeostatic plasticity of $GABA_A$ receptor mediated inhibition. J Physiol (Lond) 562: 37-46.

Montague PR, Friedlander MJ (1989) Expression of an intrinsic growth strategy by mammalian retinal neurons. Proc Natl Acad Sci U S A 86(18):7223-7227.

Montague PR, Friedlander MJ (1991) Morphogenesis and territorial coverage by isolated mammalian retinal ganglion cells. J Neurosci 11(5):1440-1457.

Niell CM, Meyer MP,Smith SJ (2004) In vivo imaging of synapse formation on a growing dendritic arbor. Nat Neurosci 7(3):254-260.

Spatkowski G, Schilling K (2003) Postnatal dendritic morphogenesis of cerebellar basket and stellate cells in vitro. J Neurosci Res 72(3):317-326.

Papa M, Segal M (1996). Morphological plasticity in dendritic spines of cultured hippocampal neurons. Neuroscience 71(4):1005-1011.

Reinecke JP, Buckner JS, Grugel SR (1980) Life-cycle of laboratory-reared tobacco hornworms, *Manduca sexta* – study of development and behaviour, using time-lapse cinematography. Biol Bull 158(1):129-140.

Schmitt S, Evers JF, Duch C, Scholz M, Obermayer K (2004) New methods for the computer-assisted 3-D reconstruction of neurons from confocal image stacks. Neuroimage 23(4):1283-1298.

Scott EK, Raabe T, Luo L (2002) Structure of the vertical and horizontal system neurons of the lobula plate in *Drosophila*. J Comp Neurol 454:470-481.

Scott EK, Reuter JE, Luo L (2003) Dendritic development of Drosophila high order visual system neurons is independent of sensory experience. BMC Neurosci 4:1-6.

Sholl DA (1953) Dendritic organisation in the neurons of the visual cortex and motor cortices of the cat. J Anat (Lond) 87:387-406

Sin WC, Haas K, Ruthazer ES, Cline HAT (2002) Dendrite growth increased by visual activity requires NMDA receptor and Rho GTPases. Nature 419(6906):475-480.

Suster ML, Bate M (2002) Embryonic assembly of a central pattern generator without sensory input. Nature 416(6877):174-178.

Somogyi P, Tamas G, Lujan R, Buhl EH (1998) Salient features of synaptic organisation in the cerebral cortex. Brain Res Brain Res Rev 26:1113-135.

Spitzer NC (1999.) New dimensions of neuronal plasticity. Nat Neurosci 2:489-491.

Suster ML, Bate M (2002) Embryonic assembly of a central pattern generator without sensory input. Nature 416:174-178.

Tessier-Lavigne M, Goodman CS (1996) The molecular biology of axon guidance. Science 274: 1123–1133.

Tolbert LP, Matsumoto SG, Hildebrandt JG (1983) Development of synapses in the antennal lobes of the moth *Manduca sexta* during metamorphosis. J Neurosci 3(6):1158-1175.

Torran-Allerand CD, Singh M, Sétáló G Jr. (1999) Novel mechanisms of estrogen action in the brain: new players in an old story. Front Neuroendocrinol 20(2):97-121.

Turrigiano GG, Nelson SB (1998) Thinking globally, acting locally: AMPA receptor turnover and synaptic strength. Neuron 21(5):933-935.

Turrigiano GG (1999). Homeostatic plasticity in neural networks: the more things change, the more they stay the same. Trends Neurosci 22:221-227.

Turrigiano GG, Nelson SB (2000) Hebb and homeostasis in neuronal plasticity. Curr Opin Neurobiol 10:358-364.

Vetter P, Roth A, Häusser M (2001). Propagation of action potentials in dendrites depends on dendritic morphology. J Neurophysiol 85(2):926-937.

Weeks JC, Levine RB (1990). Postembryonic neuronal plasticity and its hormonal control during insect metamorphosis. Annu Rev Neurosci 13:183-194.

Weeks JC, Levine RB (1995) Steroid hormone effects on neurons subserving behavior. Curr Opin Neurobiol 5(6):809-815.

Weeks JC (2003). Thinking globally, acting locally: steroid hormone regulation of the dendritic architecture, synaptic connectivity and death of an individual neuron. Prog Neurobiol 70(5):421-442.

Weliky M, Katz LC (1999) Correlational structure of spontaneous neuronal activity in the developing lateral geniculate nucleus in vivo. Science 285(5427):599-604.

West AE, Griffith EC, Greenberg ME (2002) Regulation of transcription factors by neuronal activity. Nat Rev Neurosci 3:921-931.

Wong RO, Ghosh A (2002) Activity-dependent regulation of dendritic growth and patterning. Nat Rev Neurosci 3(10):803-812.

Zhang LI, Tao HW, Poo M (2000) Visual input induces long-term potentiation of developing retinotectal synapses. Nat Neurosci 3(7):708-715.